Journal of Nuclear Medicine, published on March 30, 2017 as doi:10.2967/jnumed.117.190892

^{18}F-fluoromisonidazole kinetic modeling for characterization of tumor perfusion and hypoxia in response to antiangiogenic therapy

Milan Grkovski[1], Sally-Ann Emmas[2], Sean D. Carlin[3,4]

[1]Department of Medical Physics, Memorial Sloan Kettering Cancer Center, New York, New York, USA.

[2]Formerly Imaging, Personalised Healthcare and Biomarkers, AstraZeneca, Macclesfield, Cheshire, United Kingdom.

[3]Department of Radiology, Memorial Sloan Kettering Cancer Center, New York, New York, USA.

[4]Current Address (Corresponding Author)

Sean D. Carlin

John Morgan Building Room 168C

3620 Hamilton Walk,

University of Pennsylvania

Philadelphia, PA 19104

Word count: 5376

Abstract

Multiparametric imaging of tumor perfusion and hypoxia with ^{18}F-fluoromisonidazole (^{18}F-FMISO) dynamic positron emission tomography (dPET) may allow for an improved response assessment to antiangiogenic therapies. Cediranib (AZD2171) is a potent inhibitor of tyrosine kinase activity associated with vascular endothelial growth factor receptors-1, -2 and -3, currently in Phase II/III clinical trials. Serial ^{18}F-FMISO dPET was performed to investigate changes in tumor biomarkers of perfusion and hypoxia following cediranib treatment.

Methods: Rats bearing HT29 colorectal xenograft tumors were imaged pre-treatment (n=21) and randomized into vehicle control (0.5% methylcellulose w/v, n=9) and cediranib-treated cohorts (3mg/kg/day over 2 or 7 days (T2 and T7; n=6 in both groups)). 90-min dPET acquisitions were performed after administering 42.1±3.9 MBq of ^{18}F-FMISO by tail vein injection. Tumor volumes were delineated manually and the input function was image-derived (abdominal aorta). Kinetic modeling was carried out using an irreversible one-plasma two-tissue compartment model to estimate kinetic rate constants K_1, K_1/k_2 and k_3, surrogates for perfusion, ^{18}F-FMISO distribution volume and hypoxia-mediated entrapment, respectively. Tumor-to-blood ratios (TBR) were calculated on the last dynamic frame (80-90min). Tumors were assessed ex vivo by digital autoradiography and immunofluorescence for microscopic visualization of perfusion (pimonidazole) and hypoxia (Hoechst 33342).

Results: Cediranib treatment resulted in significant reduction of ^{18}F-FMISO mean voxelwise TBR, K_1 and K_1/k_2 in both treatment groups ($p<0.05$). The k_3 parameter was increased in both treatment groups, but only reached significance for the T2 group. No significant change in TBR, K_1, K_1/k_2 or k_3 was observed in control animals ($p>0.2$). Ex vivo tumor analysis confirmed the presence of hypoxic tumor regions that nevertheless exhibit relatively lower ^{18}F-FMISO uptake.

Conclusion: ^{18}F-FMISO kinetic modeling reveals a more detailed response to antiangiogenic treatment than a single static image. Reduced mean K_1 reflects a reduction in tumor vascular perfusion, whilst increased k_3 reflects a rise in hypoxia-mediated entrapment of the radiotracer. However, if only late static images are analyzed, the observed reduction in ^{18}F-FMISO uptake following treatment with cediranib could

be mistakenly interpreted as a global decrease, rather than increase, in tumor hypoxia. These findings support the use of ^{18}F-FMISO kinetic modeling to more accurately characterize the response to treatments that have a direct effect on tumor vascularization and perfusion.

Key words: ^{18}F-FMISO; hypoxia; perfusion; kinetic modeling; cediranib; antiangiogenesis;

Introduction

Targeting tumor neovasculature has a potential to limit cancer progression and has led to the development of antiangiogenic drugs approved for treatment of various human malignancies (1). Treatments that normalize or even promote blood vessel growth may enhance drug delivery to tumors (2) and sensitize them to chemotherapy (3). Such agents may also exacerbate hypoxia, which in turn facilitates treatment resistance by promoting neovascularization and regrowth of a more belligerent tumor phenotype (1,2), and is associated with poor overall survival (4). Recent studies aimed at alleviating tumor hypoxia while improving tumor perfusion suggest an enhanced outcome in radio-, chemo- and immunotherapies (1).

Cediranib (AZD-2171) is a novel, orally administered multi-Vascular Endothelial Growth Factor receptor (VEGFR) inhibitor (5) which is currently being tested as a maintenance treatment in patients with platinum-sensitive relapsed (PSR) ovarian cancer. Cediranib affects tumor growth by acutely impeding blood flow to the tumor, and results in a dose-dependent growth inhibition (5). However, to reach the full potential of antiangiogenic therapies, clinically relevant patient stratification is crucial. Successful implementation of window-of-opportunity trials (6) that may help select effective drug combinations for specific patients at earlier stages during treatment requires accurate monitoring of treatment response and nuanced understanding of the tumor biology.

^{18}F-fluoromisonidazole (^{18}F-FMISO) is the most widely used positron emission tomography (PET) radiotracer for non-invasive, quantitative, reproducible, and clinically feasible imaging of tumor hypoxia (7-11). However, ^{18}F-FMISO PET scans are usually performed in static mode (9), which does not allow for the simultaneous assessment of blood flow and ^{18}F-FMISO distribution volume, and may result in either underestimation or overestimation of the degree of tumor hypoxia (12). Multiparametric imaging presents an attractive opportunity for evaluating treatment response (13). Several studies have reported the added benefit of assessing both tumor perfusion and hypoxia in predicting response to therapy, suggesting that such metrics may have independent value for tumor characterization and treatment adaptation (14, 15).

Simultaneous assessment of tumor perfusion and hypoxia can be achieved through kinetic modeling of ^{18}F-FMISO dynamic PET (dPET) scans, and carries several benefits. First, uncoupling the contribution of

hypoxia-mediated entrapment to the total ^{18}F-FMISO signal results in a more accurate estimation of tumor hypoxia, since the variations in the ^{18}F-FMISO distribution volume combined with structurally and functionally abnormal vasculature may lead to low uptake in hypoxic regions or high uptake in normoxic regions even at later times post-injection (12, 16). Second, assessment of tumor perfusion is clinically relevant, as it is an indirect measure of angiogenesis, delivery of nutrients and systemic agents to the tumor, and may help in understanding response mechanisms to both systemic and targeted treatments (17). Since ^{18}F-FMISO passively diffuses out of the vasculature and through cell membranes due to its lipophilicity, early ^{18}F-FMISO uptake correlates with tumor perfusion as measured with reference standard ^{15}O-H_2O PET (18). We hypothesized that kinetic modeling of ^{18}F-FMISO dPET clarifies the ambiguity in interpreting static FMISO uptake after angiogenic therapy by decoupling the contributions of hypoxia-mediated entrapment and FMISO distribution volume to total signal.

Materials and Methods

Animal preparation, imaging and treatment

All animal experiments and procedures were approved by our Institutional Animal Care and Use Committee and complied with the National Institutes of Health regulations on the research use of rodents.

Tumor inoculation (19), ^{18}F-FMISO production (20) and dynamic PET imaging protocol (21) have been described previously. In brief, ~5.0×10^6 HT29 human colorectal carcinoma cells (ATCC Number HTB-38) were subcutaneously injected into the right hind limb of 6- to 8-week-old female athymic nu/nu rats. Animals bearing tumors between 200 and 1500mm^3 were used in the study. Animals were anesthetized with 2% isoflurane in air, and 90-min baseline dynamic PET acquisition (4×5-, 4×10-, 4×30-, 7×60-, 10×300-, and 3×600-sec frames) was initiated simultaneously with the administration of 42.1±3.9 MBq of ^{18}F-FMISO via tail vein injection. Imaging studies were performed with either an R4 or Focus 120 microPET scanner (Siemens Medical Solutions Inc.).

Subsequently, animals were randomly distributed into vehicle control (3×0.5% methylcellulose) or treatment groups (Figure 1). Treatment groups consisted of 6 animals, and the remainder assigned to the vehicle

control group. Cediranib was administered at 3.0 mg/kg/day by oral gavage (19), for either 2 or 7 days (T2 and T7 cohorts, respectively). The corresponding vehicle control cohorts are labeled as C2 and C7, respectively. The bioactivity of the selected cediranib dose (3mg/kg daily) was confirmed in our previous studies using the same tumor model system (19). After the treatment period, 90-min follow-up dynamic PET scans were performed for all groups. All animals were administered pimonidazole hydrochloride (60 mg/kg; Natural Pharmacia International, Inc.) and Hoechst 33342 (2mg in 100μl Phosphate-buffered saline; Sigma Aldrich) via tail vein at 90 and 5 minutes prior to sacrifice respectively.

Histology and autoradiography

Following imaging, animals were sacrificed and an angiocatheter placed in the tumor perpendicular to the coronal plane to preserve tumor orientation whilst sectioning. Tumors were excised and embedded in optimal-cutting-temperature mounting medium (Sakura, Finetek) frozen on dry ice, and series of 10-μm frozen sections immediately cut. To determine radiotracer distribution, digital autoradiography was performed by placing tissue sections in a film cassette against a phosphor imaging plate (Fujifilm BAS-MS2325; Fuji Photo Film) for 6 hours at −20°C. Phosphor imaging plates were read at a pixel resolution of 50μm with a BAS-1800II Bio-Imaging Analyzer (Fujifilm Medical Systems). After autoradiographic exposure, the same frozen sections were then used for fluorescence staining and microscopy.

Immunofluorescence staining for pimonidazole was performed as previously described (22) using a rabbit polyclonal anti-pimonidazole primary antibody (1:40 dilution, Cat # 2627, Natural Pharmacia International, Inc.). Secondary detection was performed using goat anti-rabbit Alexa-488 (20 μg/ml; Invitrogen) in blocking buffer. Images were acquired at ×40 magnification using a BX60 fluorescence microscope (Olympus America, Inc.) equipped with a motorized stage (Prior Scientific Instruments Ltd.) and CC12 camera (Olympus). Whole-tumor montage images were obtained by acquiring multiple fields at ×40 magnification, followed by alignment using MicroSuite Biologic Suite (version 2.7; Olympus). Sequential tumor sections were stained with Hematoxylin and eosin (H&E), and bright-field images acquired in the same manner as above.

Kinetic modeling

Voxelwise kinetic modeling of ^{18}F-FMISO dPET images was carried out in PMOD v3.604 (PMOD Technologies GmbH) using an irreversible one-plasma two-tissue compartment model (21). The analysis was focused on kinetic rate constants k_3, a surrogate for hypoxia-mediated entrapment (12, 16), K_1, a surrogate for perfusion (18), and K_1/k_2, a surrogate for ^{18}F-FMISO distribution volume. k_4 was set to 0, reflecting irreversible trapping of ^{18}F-FMISO (7). Assuming unit density tissue, k_3 and K_1 are expressed in min^{-1}, while K_1/k_2 is unitless. The image-derived input function (IDIF) was obtained by segmenting the descending aorta in the initial 3 frames of the study (0-15 sec). IDIF time activity curves (TACs) were corrected for partial volume effects and fitted with a 3-term exponential function, as described previously (21). Tumors were delineated manually on a slice-by-slice basis on the final frame (80–90 min), with tumor dimensions as measured with a caliper serving as a guideline. Tumor-to-blood ratio (TBR) was derived from the last time frame, using the measured activity concentration in the IDIF volume of interest (VOI) as the reference for blood activity concentration. Since ^{18}F-FMISO exhibits irreversible trapping, the standard Patlak formulation (23) can be used to express the TBR as

$$TBR = \frac{K_1 k_3}{k_2 + k_3} \cdot \frac{\int_0^t C_p(\tau) d\tau}{C_p(t)} + DV, \quad (1)$$

where $C_p(t)$ describes the ^{18}F-FMISO activity concentration in plasma, and DV is the ^{18}F-FMISO distribution volume, approximated by K_1/k_2. FMISO equilibration time, T^*, after which unbound FMISO has reached >99% of its final ratio relative to blood, was calculated as

$$T^* = 7 \cdot \frac{\ln(2)}{(k_2 + k_3)} \quad (2)$$

Calculation of kinetic rate constants on a voxel-level was performed using the two-tissue compartment model with ridge-regression fitting as implemented in the PXMOD tool.

Statistical analysis

Comparisons of investigated metrics between vehicle control and treated groups was performed with unpaired 2-tailed Student *t* test, assuming $p<0.05$ significance level. Pearson's correlation coefficient *r* was used to calculate the correlation between the parameters of interest.

Results

Mean animal weight and tumor volume at baseline was 216±20 g and 529±345 mm^3 respectively (n=21). Tumor volume did not significantly change in any of the four cohorts (Table 1). Analysis of static PET images (a single frame acquired between 80 and 90 minutes after ^{18}F-FMISO injection) revealed a significant reduction in mean and maximum SUV values for both the T2 and T7 cohorts relative to baseline measurements (Table 1). No significant difference was observed in either the C2 or C7 cohorts.

Kinetic modeling of ^{18}F-FMISO dynamic data revealed a more detailed picture of ^{18}F-FMISO behavior. Significant reductions in both K_1 (from 0.13 to 0.07 min^{-1}, and from 0.24 to 0.08 min^{-1} for T2 and T7 respectively) and K_1/k_2 (from 1.12 to 0.71, and from 1.21 to 0.91 for T2 and T7 respectively) were observed in the treatment groups, while no significant differences could be observed for these parameters in either of control groups (Table 2). For the k_3 parameter, a significant increase was observed in the T2 treated group (from 0.0009 min^{-1} to 0.0069 min^{-1}). An increase in the k_3 parameter in the T7 group (from 0.0039 min^{-1} to 0.0050 min^{-1}) was not significant, partially due to the wide spread of mean tumor k_3 values on the baseline scan. The latter is exemplified on the box-and-whisker plots, shown in Figure 2 for all cohorts and for all investigated kinetic rate constants. Changes in TBR mirrored the SUV data, with significant reductions observed in cediranib-treatment cohorts only (17% and 24% for T2 and T7 respectively), while differences in the C2 and C7 cohorts did not reach significance. FMISO equilibration time was found to be less than 90 min in all cohorts, confirming the sufficient length of the acquisition duration.

Representative parametric maps of TBR, k_3, K_1 and K_1/k_2 at baseline and follow-up for a cediranib-treated animal are shown in Figure 3. While the mean intratumor TBR dropped from 1.44 at baseline to 1.29 after treatment, mean intratumor k_3 (calculated by averaging the voxelwise k_3 values) increased from 0.0022 min^{-1} to 0.0069 min^{-1}, indicating an actual increase in hypoxia-mediated entrapment of ^{18}F-FMISO. Decrease in TBR can be explained by both decreased perfusion due to pruning of intratumor vessels (mean intratumor K_1 dropped from 0.15 min^{-1} to 0.08 min^{-1}) and lower ^{18}F-FMISO distribution volume (mean intratumor K_1/k_2 dropped from 1.16 to 0.86).

The discordance between k_3 and TBR as surrogate markers for tumor hypoxia is further highlighted in k_3-TBR scatterplots for two animals, one from a treated cohort (T7; Fig. 4A), and the other from a control

cohort (C2; Fig. 4B). While in the control animal, Pearson's *r* between voxelwise values of k_3 and TBR is high and remains relatively unchanged (decreasing from 0.85 to 0.73), the corresponding *r* in the treated animal decreases substantially from 0.65 at baseline to -0.45 after treatment. Of note, the decrease in TBR in the latter case was not due to decrease in k_3 or long ^{18}F-FMISO equilibration time, but due to lower ^{18}F-FMISO distribution volume. Results confirming the foregoing observations were observed when the k_3-TBR correlation was calculated on a whole tumor level (i.e., by taking mean voxelwise k_3 and TBR for each animal). Pearson's *r* changed from 0.63 to 0.51 in control animals (to achieve higher statistics, C2 and C7 cohorts were pooled into a single cohort), while for treated animals (pooled data including both T2 and T7 cohorts), it changed substantially, from 0.66 to -0.39.

Ex vivo analysis of tumor sections provided further detail regarding the distribution of ^{18}F-FMISO in the treatment and control cohorts. Representative examples of co-registered images showing ^{18}F-FMISO digital autoradiographs (DAR), immunofluorescence staining (IF) and H&E staining are shown for HT29 xenograft tumors excised from treated and control animals (Fig. 5 and Supplementary Fig. S1). The tumors were generally characterized by largely necrotic centers containing 'islands' of viable cells (seen on H&E), well-perfused rims (evidenced by Hoechst 33342 staining, blue), and an extensive perinecrotic hypoxic region staining positive for the exogenous hypoxia tracer pimonidazole (green). In the control cohort tumors, ^{18}F-FMISO distribution closely corresponded to the spatial pattern of pimonidazole uptake. Islands of viable tumor approximate to the boundary of the necrotic region were clearly visualized by pimonidazole immunofluorescence staining, and also by ^{18}F-FMISO DAR. Analysis of tumors from the cediranib-treated cohorts revealed some notable differences from the control tumors. There was a loss of correspondence between pimonidazole staining in some, generally centrally-located tumor regions, with these regions characterized by strong pimonidazole staining, but weak or absent staining for Hoechst 33342. Also of note was the absence of ^{18}F-FMISO uptake in these regions. In contrast, the peripheral regions of these tumors generally showed a strong correspondence between ^{18}F-FMISO uptake and pimonidazole staining. The non-correspondence of pimonidazole and ^{18}F-FMISO in the cediranib-treatment groups is explained by the large differences in the concentrations administered (approximately 220μM and 4.8 pM for pimonidazole and ^{18}F-FMISO respectively), greatly reducing the sensitivity of pimonidazole to changes in tracer delivery relative to ^{18}F-FMISO.

Discussion

This study was carried out to explore the use of ^{18}F-FMISO as an imaging biomarker for the acute effects of antiangiogenic therapies, and to investigate which imaging metrics most accurately reflect the underlying changes in tumor physiology caused by these treatments. Sustained angiogenesis is one of the hallmarks of cancer, and the targeting and exploitation of tumor neovasculature provides an additional pharmaceutical option for disease management. However, many antiangiogenic drugs have a complex effect on tumor blood supply and oxygen delivery, with an acute reduction in tumor perfusion, followed by a longer process of vascular normalization (24). This initial effect may facilitate an acute hypoxic response, in turn fueling tumor progression (1), and may have important implications for the optimal scheduling of concurrent radiation therapy. Accurate characterization of tumor perfusion and hypoxia may therefore prove to be an important consideration for patient stratification prior to therapy and for treatment modification after the onset of therapy.

^{18}F-FMISO PET is the most extensively evaluated technique for non-invasive, quantitative imaging of tumor hypoxia (9). Bartlett and colleagues, working with a prostate-tumor model, concluded that kinetic modeling of ^{18}F-FMISO dPET data provides additional information otherwise unavailable from static images, and that the k_3 parameter is better at identifying low tissue oxygen than other measures of ^{18}F-FMISO uptake (16). Recently, we demonstrated that kinetic modeling of ^{18}F-FMISO dPET data can clarify the ambiguity in interpreting the static ^{18}F-FMISO uptake in patients with head and neck cancer (12).

The presented findings support the conclusion of the foregoing study, indicating that kinetic modeling of ^{18}F-FMISO dPET data allows for a more detailed response assessment to an antiangiogenic agent than can be achieved through a single static image. The observation of decreased total ^{18}F-FMISO SUV relative to baseline (Table 1) implies a cediranib-mediated reduction in tumor hypoxia. However, kinetic analysis revealed that in at least a fraction of tumor voxels, the rate of hypoxia-specific entrapment of ^{18}F-FMISO (k_3) actually increases (Table 2 and Figure 2). We also observed a large drug-dependent reduction in vascular delivery of ^{18}F-FMISO (K_1), which reflects similar reductions we and others have observed in delivery of gadolinium contrast agent, measured using dynamic magnetic resonance imaging (25, 26), as well as reductions in ^{18}F-FMISO distribution volume as reflected by K_1/k_2, which may reflect the higher

fraction of necrotic cells after the treatment. Parametric mapping revealed heterogeneous responses to cediranib, with voxels showing global reduction in K_1 and K_1/k_2, whilst those with higher k_3 tended to be seen in more centrally-located tumor regions (Figure 3).

While for control animals, k_3 and TBR were relatively well correlated, both on a voxel-by-voxel as well as on a whole-tumor level, treatment with cediranib decreased the k_3-TBR correlation substantially (Figure 4). These results indicate that in cases when antiangiogenic drugs are administered, static ^{18}F-FMISO uptake metrics might not reflect the underlying hypoxia status accurately. TBR depends not only on k_3, but also on K_1/k_2 (^{18}F-FMISO distribution volume) and T* (^{18}F-FMISO equilibration time). By pruning the tumor vessels and increasing the fraction of non-viable tumor cells (causing reduced K_1/k_2), ^{18}F-FMISO might appear to decrease after antiangiogenic therapy despite constant or even increasing levels of tumor hypoxia, leading to an incorrect assessment of tumor response. Note that under normoxic conditions (k_3=0), TBR will reflect the ^{18}F-FMISO distribution volume (Equation 1). Consequently, K_1/k_2 has a potential to bias the assessment of ^{18}F-FMISO uptake if only static scans are used (12). For treated animals, K_1/k_2 values were consistently lower than 1, resulting in lower TBR values that underestimate the degree of intratumor hypoxia. FMISO equilibration time was found to be less than 90 min in all cohorts, therefore lower total FMISO uptake was not caused by tumor hypoperfusion.

The foregoing observations are supported by ex vivo digital autoradiography and immunofluorescence staining of tumor sections. In non-treated control animals, an inverse relationship with the vascular perfusion marker Hoechst 33342 was found for areas staining positive for pimonidazole. ^{18}F-FMISO autoradiography exhibited a strong positive correspondence with pimonidazole uptake as expected. In the cediranib-treated animals, many of the centrally-located regions of viable tissue did not show significant accumulation of ^{18}F-FMISO, despite showing uptake of pimonidazole. ^{18}F-FMISO signal was observed mainly in the tumor periphery, localized adjacent to regions of high Hoechst 33342 staining, without the clear correspondence with pimonidazole seen in the control tumors. These distributions imply that uptake of ^{18}F-FMISO in the central tumor region is reduced even though these regions remain hypoxic, and reflects the reduced K_1 and elevated k_3 parameters as observed from kinetic modeling.

Whilst pimonidazole and ^{18}F-FMISO were co-administered approximately 90 minutes before sacrifice, these similarly-structured hypoxia tracers provided divergent information in the cediranib-treatment groups. This can be explained by the high molar concentration of pimonidazole administered (approximately 220μM), and the binary nature of the immunofluorescence-based detection of pimonidazole adducts rendering the pimonidazole-based identification of hypoxic tumor regions much less sensitive to fluctuations in vascular tracer delivery than ^{18}F-FMISO, where a much lower concentration is given (approximately 4.8 pM), and the absolute tracer uptake is measured. Whilst differences in the respective pO_2 sensitivity of the hypoxia tracers, and the potential for a partial volume effect to reduce apparent ^{18}F-FMISO activity are also possible explanations for this observation, there is no observation of either effect in the control tumors, suggesting that the influence of these phenomena is likely to be small.

The results presented in this study go some way to explain the divergent and occasionally confounding data regarding the effect of antiangiogenic agents on tumor hypoxia and ^{18}F-FMISO imaging response. There are multiple reports of observations that antiangiogenic agents can increase tumor hypoxia by promoting vessel pruning and inhibiting neo-angiogenesis (27-29), often determined using IHC markers of tumor hypoxia. In contrast, there are also several reports of a reduction in ^{18}F-FMISO uptake following antiangiogenic treatment (30-34). Differences in the antiangiogenic compounds, tumor types and experimental methodologies used make it difficult to draw a definitive conclusion. However, our data suggests that whilst metrics derived from static scans are attractive due to the simple image acquisition protocols, ^{18}F-FMISO uptake may not directly reflect changes in intratumor hypoxia, unless radiotracer delivery and distribution is also accounted for. For this reason, we believe that the use of dynamic acquisition protocols should be considered in instances where tumor perfusion and tracer distribution is directly affected by the treatment under evaluation. Clarifying the relative contributions of tracer distribution, tumor perfusion and tumor hypoxia to total ^{18}F-FMISO signal yields multiparametric imaging data that can help to better understand the acute response and mechanisms of resistance to antiangiogenic therapy, and may better inform optimal drug dosing and treatment scheduling.

Conclusion

^{18}F-FMISO kinetic modeling reveals a more detailed response to cediranib treatment than a single static image. Reduced mean K_1 reflects a reduction in vascular perfusion, whilst increased k_3 reflects a rise in hypoxia-mediated tracer entrapment. However, if only late static images from the same dataset are analyzed, the reduction in ^{18}F-FMISO uptake following cediranib treatment could be mistakenly interpreted as a global decrease, rather than increase, in tumor hypoxia. These findings support the use of ^{18}F-FMISO kinetic modeling to more accurately characterize the response to treatments that have a direct effect on tumor vascularization and perfusion.

DISCLOSURES

S-A.E. is a former employee of AstraZeneca.

ACKNOWLEDGEMENTS

Services provided by the MSKCC Radiochemistry and Molecular Imaging Probes Core Facility were supported in part by NIH grant P30 CA008748 (P.I. Craig Thompson). Dr Carlin is also partially funded by a generous grant from the Mesothelioma Applied Research Foundation.

References

1. Jain RK. Antiangiogenesis strategies revisited: from starving tumors to alleviating hypoxia. *Cancer Cell*. 2014;26:605-622.

2. Rivera LB, Bergers G. Tumor angiogenesis, from foe to friend. *Science*. 2015;349:694-695.

3. Wong PP, Demircioglu F, Ghazaly E, et al. Dual-action combination therapy enhances angiogenesis while reducing tumor growth and spread. *Cancer Cell*. 2015;27:123-137.

4. Horsman MR, Mortensen LS, Petersen JB, Busk M, Overgaard J. Imaging hypoxia to improve radiotherapy outcome. *Nat Rev Clin Oncol.* 2012;9:674-687.

5. Wedge SR, Kendrew J, Hennequin LF, et al. AZD2171: a highly potent, orally bioavailable, vascular endothelial growth factor receptor-2 tyrosine kinase inhibitor for the treatment of cancer. *Cancer Res*. 2005;65:4389-4400.

6. Dubois LJ, Niemans R, van Kujik SJ, et al. New ways to image and target tumour hypoxia and its molecular responses. *Radiother Oncol*. 2015;116:352-357.

7. Koh WJ, Rasey JS, Evans ML, et al. Imaging of hypoxia in human tumors with [F-18]fluoromisonidazole. *Int J Radiat Oncol Biol Phys.* 1992;22:199-212.

8. Rasey JS, Koh WJ, Evans ML, et al. Quantifying regional hypoxia in human tumors with positron emission tomography of [18F]fluoromisonidazole: a pretherapy study of 37 patients. *Int J Radiat Oncol Biol Phys.* 1996;36:417-428.

9. Fleming IN, Manavaki R, Blower PJ, et al. Imaging tumour hypoxia with positron emission tomography. *Br J Cancer*. 2015;112:238-250.

10. Okamoto S, Shiga T, Yasuda K, et al. High reproducibility of tumor hypoxia evaluated by 18F-fluoromisonidazole PET for head and neck cancer. *J Nucl Med* 2013;54:201-207.

11. Grkovski M, Schwartz J, Rimner A, et al. Reproducibility of 18F-fluoromisonidazole intratumour distribution in non-small cell lung cancer. *EJNMMI Res* 2016;6:79.

12. Grkovski M, Lee NY, Schöder H, et al. Multiparametric imaging of tumor hypoxia and perfusion with 18F-fluoromisonidazole dynamic PET in head and neck cancer. *J Nucl Med* February 9, 2017. doi: 10.2967/jnumed.116.188649 [Epub ahead of print].

13. Padhani AR, Miles KA. Multiparametric imaging of tumor response to therapy. *Radiology*. 2010;2:348-364.

14. Lehtiö K, Eskola O, Viljanen T, et al. Imaging perfusion and hypoxia with PET to predict radiotherapy response in head-and-neck cancer. *Int J Radiat Oncol Biol Phys.* 2004;59:971-982.

15. Thorwarth D, Eschmann SM, Scheiderbauer J, Paulsen F, Alber M. Kinetic analysis of dynamic 18F-fluoromisonidazole PET correlates with radiation treatment outcome in head-and-neck cancer. *BMC Cancer*. 2005;5:152.

16. Bartlett RM, Beattie BJ, Naryanan M, et al. Image-guided PO2 probe measurements correlated with parametric images derived from 18F-fluoromisonidazole small-animal PET data in rats. *J Nucl Med*. 2012;53:1608-1615.

17. Rajendran JG, Mankoff DA. Positron Emission Tomography Imaging of Blood Flow and Hypoxia in Tumors. In Shields, AF., Price P. *In vivo imaging of cancer therapy*. Springer Science & Business Media, 2007.

18. Bruehlmeier M, Roelcke U, Schubiger PA, Ametamey SM. Assessment of hypoxia and perfusion in human brain tumors using PET with 18F-fluoromisonidazole and 15O-H2O. *J Nucl Med*. 2004;45:1851-1859.

19. Bokacheva L, Kotedia K, Reese M, et al. Response of HT29 colorectal xenograft model to cediranib assessed with 18F-fluoromisonidazole positron emission tomography, dynamic contrast-enhanced and diffusion-weighted MRI. *NMR Biomed.* 2013;26:151-163.

20. Lim JL, Berridge MS. An efficient radiosynthesis of [18F]fluoromisonidazole. *Appl Radiat Isot. 1993*;44:1085–1091.

21. Grkovski M, Schwartz J, Gönen M, et al. Feasibility of 18F-Fluoromisonidazole Kinetic Modeling in Head and Neck Cancer Using Shortened Acquisition Times. *J Nucl Med*. 2016;57:334-341.

22. Carlin S, Zhang H, Reese M, et al. A comparison of the imaging characteristics and microregional distribution of 4 hypoxia PET tracers. *J Nucl Med*. 2014;55:515-521.

23. Patlak CS, Blasberg RG. Graphical evaluation of blood-to-brain transfer constants from multiple-time uptake data. Generalizations. J Cereb Blood Flow Metab. 1985;5:584-590.

24. Jain RK, Duda DG, Willett, CG, et al., Biomarkers of response and resistance to antiangiogenic therapy. *Nat Rev Clin Oncol.* 2009;6:327-338.

25. Bradley DP, Tessier JL, Checkley D, et al., Effects of AZD2171 and vandetanib (ZD6474, Zactima) on haemodynamic variables in an SW620 human colon tumour model: an investigation using dynamic contrast-enhanced MRI and the rapid clearance blood pool contrast agent, P792 (gadomelitol). *NMR Biomed*. 2008;21:42-52.

26. Bradley DP, Tessier JJ, Lacey T, et al., Examining the acute effects of cediranib (RECENTIN, AZD2171) treatment in tumor models: a dynamic contrast-enhanced MRI study using gadopentate. *Magn Reson Imaging*. 2009;27:377-384.

27. Rapisarda A, Melillo G, Overcoming disappointing results with antiangiogenic therapy by targeting hypoxia. *Nat Rev Clin Oncol.* 2012;9:378-390.

28. Ulivi P, Marisi G, Passardi A, Relationship between hypoxia and response to antiangiogenic therapy in metastatic colorectal cancer. *Oncotarget*, 2016 Apr 12. doi: 10.18632/oncotarget.8172 [Epub ahead of print].

29. Pham E, Yin M, Peters CG, et al., Preclinical Efficacy of Bevacizumab with CRLX101, an Investigational Nanoparticle-Drug Conjugate, in Treatment of Metastatic Triple-Negative Breast Cancer. *Cancer Res*, 2016;76:4493-4503.

30. Thézé B, Bernards N, Beynel A, et al., Monitoring therapeutic efficacy of sunitinib using [(18)F]FDG and [(18)F]FMISO PET in an immunocompetent model of luminal B (HER2-positive)-type mammary carcinoma. *BMC Cancer*, 2015;7:534

31. Hernández-Agudo E, Mondejar T, Soto-Montenegro ML, et al., Monitoring vascular normalization induced by antiangiogenic treatment with (18)F-fluoromisonidazole PET. *Mol Oncol*. 2016;10:704-718.

32. Diaz R, Nguewa PA, Redardo M, Manrique I, Calvo A, Sunitinib reduces tumor hypoxia and angiogenesis, and radiosensitizes prostate cancer stem-like cells. *Prostate*. 2015;75:1137-1149.

33. Valable S, Petit E, Roussel S, et al., Complementary information from magnetic resonance imaging and (18)F-FMISO positron emission tomography in the assessment of the response to an antiangiogenic treatment in a rat brain tumor model. *Nucl Med Biol.* 2011;38:781-793.

34. Hugonnet F, Fournier L, Medioni J, et al. Metastatic renal cell carcinoma: relationship between initial metastasis hypoxia, change after 1 month's sunitinib, and therapeutic response: an 18F-fluoromisonidazole PET/CT study. *J Nucl Med*. 2011;52:1048-1055.

FIGURES

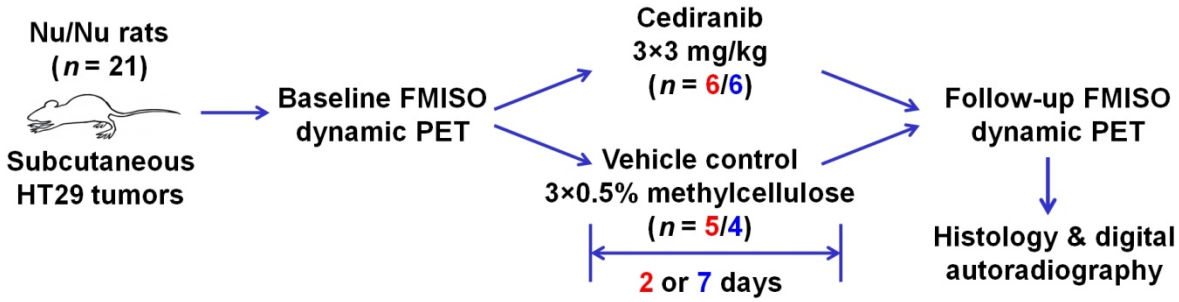

Figure 1. Experimental schematic. Animals with colorectal carcinoma-bearing tumor xenografts were imaged with ^{18}F-FMISO dynamic PET at baseline and subsequently randomized in treatment and vehicle control groups. After the treatment period, second ^{18}F-FMISO dynamic PET scans were performed, followed by ex vivo analysis of tumor specimens.

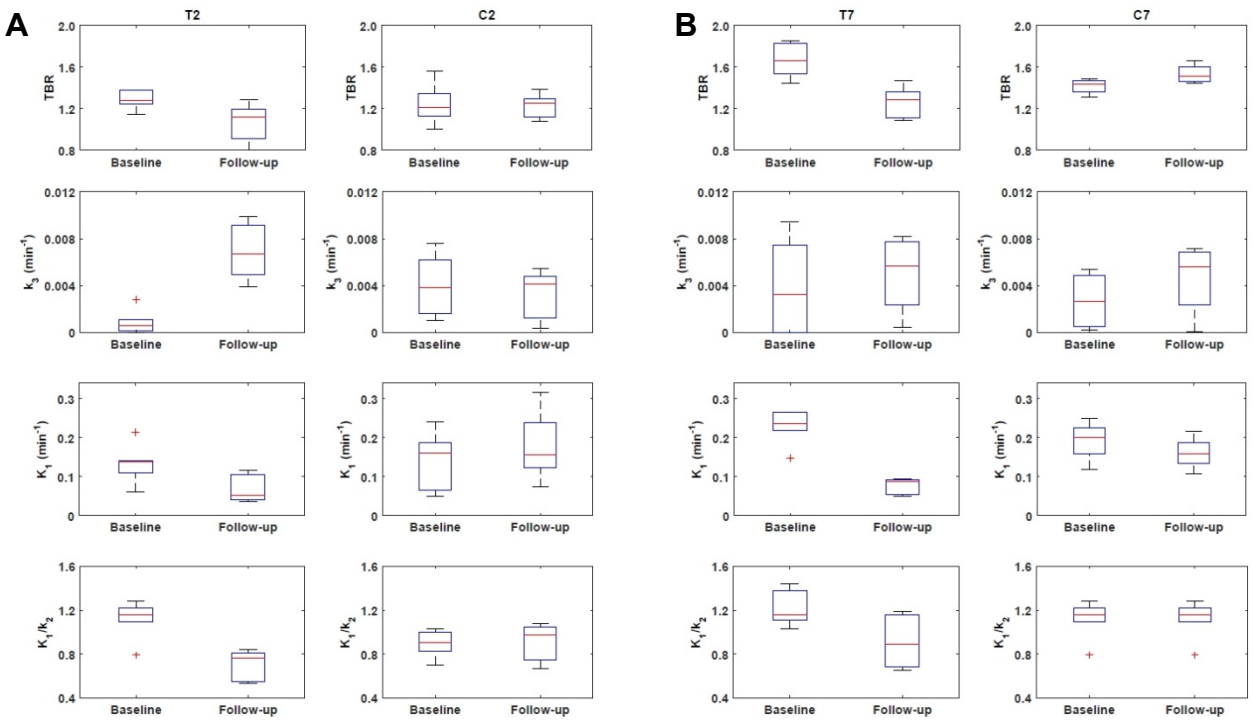

Figure 2. (A) Box-and-whisker plots summarizing mean intratumor values of Tumor-to-Blood Ratio, k_3, K_1 and K_1/k_2 (from top to bottom row), for animals treated for 2 days with cediranib (T2; left panel), and vehicle control group (C2; right panel). (B) Corresponding plots for animals treated for 7 days with cediranib (T7; left panel), and vehicle control group (C7; right panel).

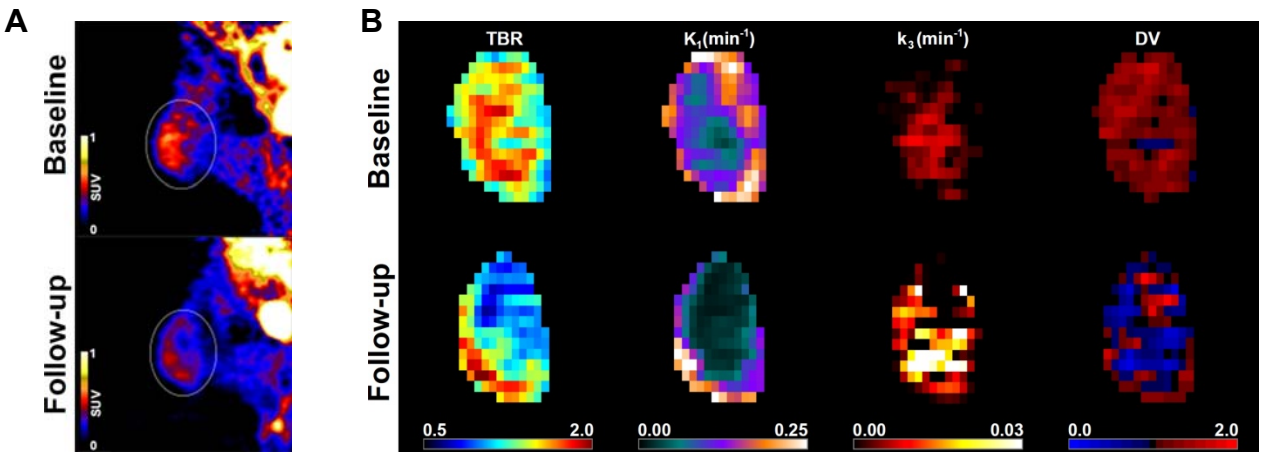

Figure 3. (A) Single-slice, mid-tumor PET images obtained at 90 minutes post-injection from a representative animal in the T7 cohort at baseline (left) and following 7 days of cediranib treatment (right). (B) Intratumor voxel-wise maps (coronal view) derived from dynamic PET images from the same animal, obtained at baseline (top row), and following 7 days of cediranib treatment (bottom row). Parameters shown are tumor-to-blood radio (TBR), K_1 and k_3.

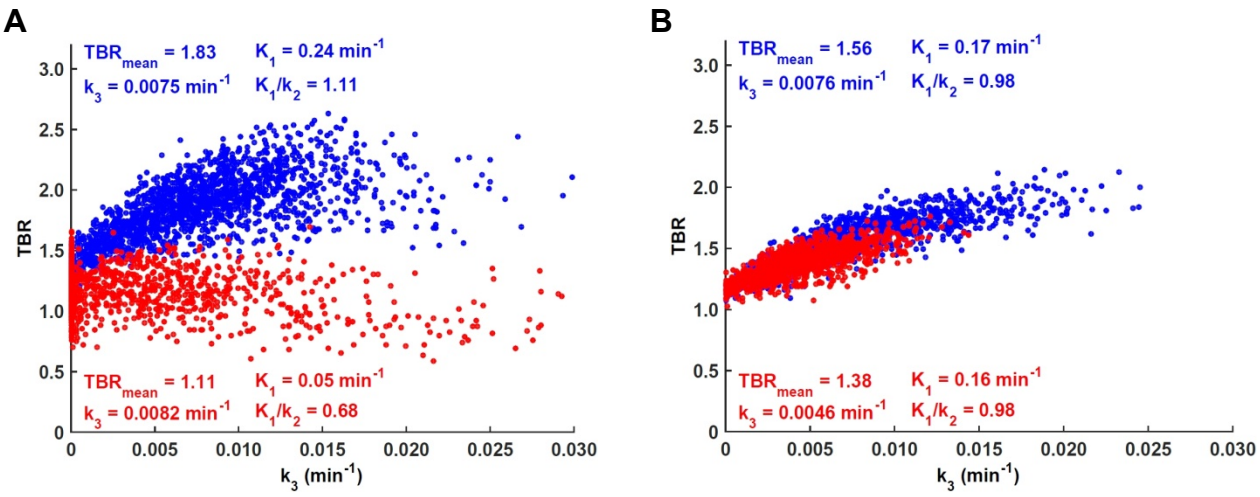

Figure 4. (A) Correlation between k_3 and Tumor-to-Blood Ratio (TBR), two surrogate markers of tumor hypoxia, for a representative animal treated with cediranib (T7 cohort). Pearson's *r* between k_3 and TBR changed substantially, from 0.65 at baseline (blue) to -0.45 at follow-up (red) ^{18}F-FMISO scan, while T* increased from 22 min to 60 min, respectively. (B) Corresponding scatterplot for a representative vehicle-control animal (C2 cohort). Pearson's *r* between k_3 and TBR changed only slightly, from 0.85 at baseline (blue) to 0.73 at follow-up (red) ^{18}F-FMISO scan, while T* remained relatively unchanged (27 min and 29 min, respectively).

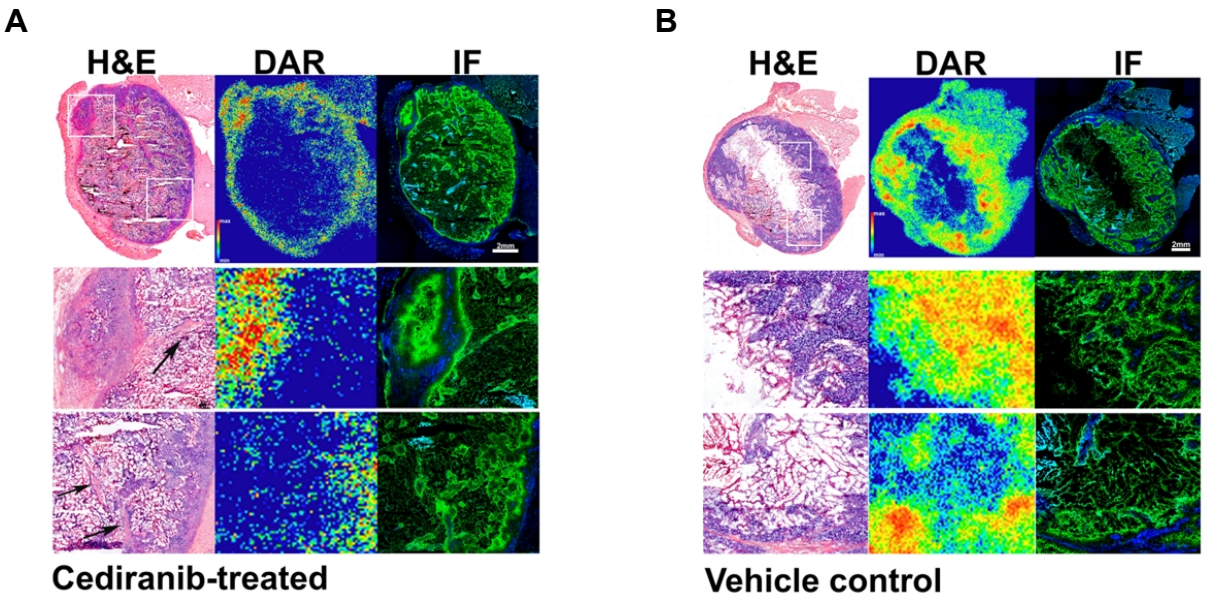

Figure 5. Haematoxylin and Eosin (H&E), digital autoradiography (DAR) and immunofluorescence (IF, green – pimonidazole, blue – Hoechst 33342) analysis of ex-vivo tumor sections. Upper and lower zoom regions indicated on whole-mount H&E image. (A) Cediranib-treated tumors showed viable central regions positive for pimonidazole, but lacking ^{18}F-FMISO uptake (indicated by black arrows). (B) Control tumors showed a strong correspondence between pimonidazole staining and ^{18}F-FMISO uptake in both central and peripheral regions.

TABLES

Table 1. Summary of tumor volume, and mean and maximum standardized uptake values (SUV) obtained at baseline (pre) and follow-up (post) in cohorts treated with cediranib or vehicle for 2 and 7 days.

	Volume (mm^3)		SUV_{mean}		SUV_{max}	
	Pre	Post	Pre	Post	Pre	Post
			2 day cohort			
Cediranib (n=6)	330±63	345±53	0.52±0.04	0.39±0.08	0.96±0.09	0.73±0.18
	p=0.67		p=0.01*		p=0.03*	
Control (n=5)	526±378	518±422	0.53±0.05	0.49±0.07	1.05±0.15	1.00±0.20
	p=0.98		p=0.11		p=0.36	
			7 day cohort			
Cediranib (n=6)	700±297	604±248	0.56±0.17	0.38±0.08	0.99±0.32	0.71±0.19
	p=0.56		p=0.01		p=0.01*	
Control (n=4)	577±556	931±982	0.58±0.18	0.52±0.21	1.07±0.31	0.92±0.46
	p=0.55		p=0.40		p=0.30	

*Statistical significance. SUV - standardized uptake value.

Table 2. Summary of ^{18}F-FMISO kinetic modeling before and after cediranib treatment.

	K_1 (min^{-1})		k_3 (min^{-1})		K_1/k_2		TBR_{mean}		T* (min)	
	Pre	Post	Pre	Post	Pre	Post	Pre	Post	Pre	Post
2 day cohort										
Treated (n=6)	0.13± 0.05	0.07± 0.03	0.0009± 0.0011	0.0069± 0.0023	1.12± 0.17	0.71± 0.13	1.28± 0.09	1.06± 0.20	44±12	58±25
	p=0.02*		p<0.01*		p<0.01*		p=0.03*		p=0.24	
Control (n=5)	0.14± 0.08	0.17± 0.09	0.0040± 0.0027	0.0032± 0.0022	0.90± 0.13	0.91± 0.18	1.24± 0.20	1.22± 0.12	40±21	29±14
	p=0.46		p=0.62		p=0.51		p=0.87		p=0.39	
7 day cohort										
Treated (n=6)	0.24± 0.07	0.08± 0.02	0.0039± 0.0039	0.0050± 0.0032	1.21± 0.16	0.91± 0.23	1.66± 0.16	1.27± 0.15	25±6	55±7
	p<0.01*		p=0.60		p=0.02*		p<0.01*		p<0.01*	
Control (n=4)	0.19± 0.05	0.16± 0.04	0.0027± 0.0026	0.0046± 0.0032	1.18± 0.15	1.14± 0.19	1.42± 0.07	1.53± 0.10	32±6	34±4
	p=0.40		p=0.39		p=0.78		p=0.11		p=0.65	

*Statistical significance. TBR - Tumor-to-Blood Ratio.

Supplementary Data

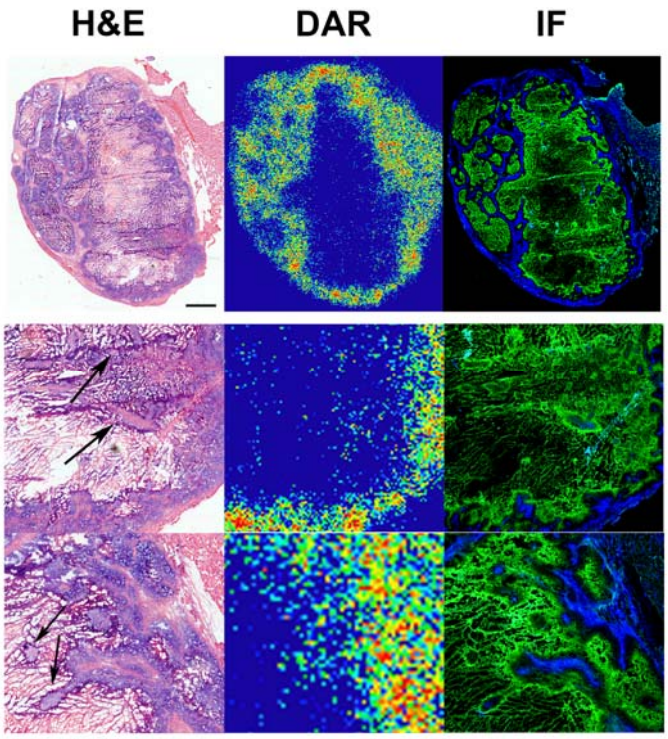

Supplementary Figure 1. Additional examples of ex vivo analysis of cediranib-treated (left panel) and control (right panel) tumors. Haematoxylin and Eosin (H&E), digital autoradiography (DAR) and immunofluorescence (IF, green – pimonidazole, blue – Hoechst 33342) is shown. Control tumors showed a strong correspondence between pimonidazole staining and ^{18}F-FMISO uptake in both central and peripheral regions. Cediranib-treated tumors showed viable central regions positive for pimonidazole, but lacking ^{18}F-FMISO uptake (indicated by black arrows).